



## Journal of Advanced Research in Applied Sciences and Engineering Technology

Journal homepage:  
[https://semarakilmu.com.my/journals/index.php/applied\\_sciences\\_eng\\_tech/index](https://semarakilmu.com.my/journals/index.php/applied_sciences_eng_tech/index)  
ISSN: 2462-1943



# Analysis, Modelling and Simulation for the Intelligent Active Vibration Control of a Combined Plant using a New Gyroscopic Combined Actuator Model

Abbas Moloody<sup>1</sup>, Azizan As'arry<sup>1,\*</sup>, Tang Sai Hong<sup>1</sup>, Raja Kamil<sup>2</sup>, Irfan Bahiuddin<sup>3</sup>

- <sup>1</sup> Department of Mechanical and Manufacturing Engineering, Faculty of Engineering, Universiti Putra Malaysia (UPM), 43400 Serdang, Selangor, Malaysia  
<sup>2</sup> Department of Electrical and Electronics Engineering, Faculty of Engineering, Universiti Putra Malaysia (UPM), 43400 Serdang, Selangor, Malaysia  
<sup>3</sup> Department of Vocational College, Universitas Gadjah Mada (UGM), Sleman Regency, Special Region of Yogyakarta 55281, Indonesia

### ABSTRACT

There have been several research conducted worldwide on analysis, modelling, and controlling for flexible manipulator architectures. In this paper, one of the most interesting areas in the science of rotational dynamics as the study of spinning solid objects, such as Gyroscopes (G) has been investigated as a new approach for the improvement of the gyroscope non-linear behaviour which controls the magnitude and the direction of the torque separately in the frequency domain by describing a New Graphical Combined Actuator Model (NGCAM) for the Intelligent Active Vibration Control (IAVC) of a Combined Plant (CP) as a linear-nonlinear combined single link Robotics Flexible Manipulator (RFM) structure which rotates in the horizontal plane with two degrees of freedom in order to have a performance assessment and suppressing vibrations. The effect of the parameter variation on the stability and dynamic nonlinear behaviour of the gyroscope in gimbals with a feedback sensor control system has been formed and optimized by the Modified Fuzzy Logic (MFL) algorithm as an artificial intelligence control technique and the Proportional, Integral and Derivative (PID) tuning by the modified Ziegler Nichols (ZN) method. To validate the gyroscope stabilization to be implemented into the RFM for controlling the vibration, the proposed method combines Active Force Control (AFC) technique with Fuzzy Logic (FL) and PID as the (AVC-FL-PID) controller for the NGCAM, CP and RFM by using MATLAB & SIMULINK program is created. For a linear-non-linear combination system, it is better to use a linear-non-linear combination controller. Simulation results illustrate the effectiveness of the proposed strategy which is significantly and quite satisfactory about 25 (%) generally better than compared to the other systems' performance criteria and is so clear and significant optimization is visible than compared to the other conventional actuators such as PZTs and other control strategies in improvement stabilization and vibration control of RFM structures. The advantages of the proposed method and the possibilities of further improvements are discussed.

### Keywords:

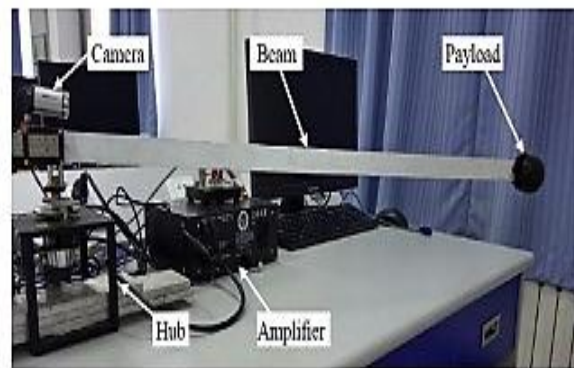
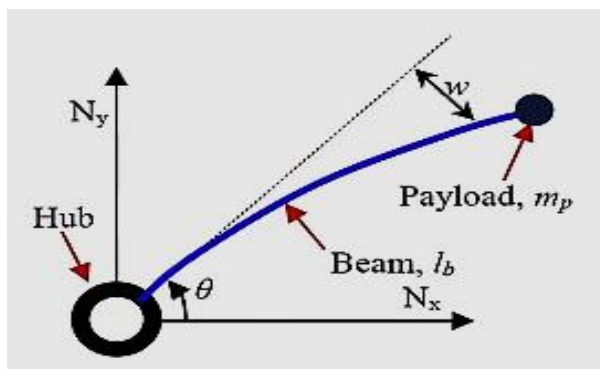
Intelligent active vibration control;  
Combined plant; New graphical  
combined actuator model; Flexible  
manipulator; Gyroscope

\* Corresponding author.  
E-mail address: zizan@upm.edu.my

## 1. Introduction

Since they are widely employed in engineering science and scientific research applications, such as space exploration, undersea surveys, industrial and military sectors, welding, painting, assembly, and medical applications, mechatronics and robotics domains and systems have drawn an increasing amount of interest from researchers in recent years. Robotic and mechatronic manipulators are multi-segment devices that are electronically controlled and interact with their surroundings to carry out tasks. Other names for them are industrial manipulators and industrial arms. These manipulators are widely utilized in the industrial production industry and have a variety of specialized uses (the Canadarm, for instance, was used to maneuver cargo on space shuttles). Many of these arms and manipulators are built and developed in a way that will enhance strength and minimize the consequences of mechanical vibrations at the robot's end (End Effector). The performance of many industrial processes is frequently constrained by the vibration of the structure, which can result in structural damage, fatigue, instability, and poor performance by Tavakolpour *et al.*, [1]. In construction, vibrations are an unwanted event. The undesirable vibration may cause structural damage or adversely affect system operation. The simplest solution for mitigating vibration is to create the structure stiffer, although this adds weight and is not always appropriate or acceptable. Utilizing passive vibration control technology, such as vibrating absorbers or dynamic absorbers that are passively attached, is another common tactic. Passive solutions may not be ideal in many situations since it is preferable to keep the weight as low as feasible by Christopher *et al.*, [2]. For the vibration suppression of this typically complicated system, much study has been done. The conventional approach to making these manipulators stiffer and preventing mechanical vibration in the end effectors is to use heavy materials and bulky designs. The intricacy of flexible structures has prevented conventional control systems from being universally effective. Furthermore, because these structures often have low frequencies, vibration control becomes a significant problem. The drawbacks of the heavy rigid manipulators employed by most existing robotic manipulators are their high-power consumption, slow motion, danger, and lower productivity by Dwived and Eberhard *et al.*, [3]. Recently, there has been a significant increase in demand for flexible robots that move faster and use less energy. Therefore, a great deal of research on analysis, modelling, and controlling for flexible manipulators has been done globally by Sayahkarajy *et al.*, [4]. Flexible constructions invariably run the risk of performing poorly owing to mechanical vibration, which would negatively impact the industrial system by Kotnik, Yurkovich and Ozguner [5]. Because of this, despite much effort, controlling flexible manipulators is still a difficult task. Rigid Manipulators (RM) and Flexible Manipulators (FM) are two main categories into which these manipulators have been separated. The development of approaches for the modelling and control of robot flexible manipulator systems has been the subject of extensive study. In the 1970s, work on the dynamics, mathematical modelling, analysis, and control of the flexible mechanism really got going. Feedback control strategies have been researched for precise positioning and vibration management of single link flexible robotic manipulators due to the complexity of multi-link manipulator systems. These techniques include integral resonance control by Pereira *et al.*, [8]. Lyapunov-based control by Pereira, Aphale, Feliu and Moheimani [7] and pole placement by Ge, Lee and Zhu [6]. According to Preumont [9], the controllers for flexible manipulators must achieve the same motion target as the controllers for rigid manipulators while also stabilizing the vibrations. The best potential vibration suppression for flexible manipulators has been achieved with AVC. Researchers and engineers are using smart material as an alternative approach to aid increase control performance in the AVC experiments. Since smart materials are frequently small, light, responsive, and may include flexible components, they are more desired by

Chen and Astolfi [10]. Flexible robot manipulator systems may be controlled using intelligent control that is based on neural networks (NN), fuzzy logic (FL), and evolutionary algorithms. It has taken a tremendous amount of work to create and deploy NN-based controllers for flexible manipulators. Chen and Wen suggested a neural controller and observer to direct a flexible manipulator to a desired trajectory using hub position and velocity information [11]. However, in this study, only linear models are permitted by Donne and Ozguner [12]. The control of a single-link flexible manipulator whose dynamics are only partially understood has been considered by Donne and Ozguner. This work, which is thought to be the first in the study of a gyroscope system, hasn't been covered in a literature review as far as the author is aware. The purpose of the study is to discuss the efficacy of specified gyroscope models that are used to simulate their non-linear dynamics. The gyroscope flywheel will rotate around the ( $\omega$ ) axis throughout this study article. The flywheel will also be gimbaled about the ( $\alpha$ ) axis, and the system will experience instabilities about the ( $\theta$ ) axis. Hence, as a nonlinear device the gyroscope performance has been studied and based on the behaviour, a mode with suitable function has been proposed and developed based on the proper function of the system and defining a New Graphical Combined Actuator Model (NGCAM) attached on the main plant consists of a spinning wheel with two degrees of freedom, rotation about a vertical axis (spin) and a rotation about a horizontal axis (precession) and a characteristic inertia, damping and stiffness for the Intelligent Active Vibration Control (IAVC) of a Combined Plant (CP) as a linear-nonlinear combined single link Robotics Flexible Manipulator (RFM) structure which rotates in the horizontal plane with two degrees of freedom in order to improve the behaviours of CP or RFM as the system, the gyroscopic stabilization and controlling the vibration. In general, loads are picked up and transferred to particular locations using the Robotics Flexible Manipulator (RFM) framework. In comparison to Robotics Rigid Manipulator (RRM), it provides several benefits, including quick reaction, reduced energy consumption, less weight, the need for fewer actuators, cheaper total cost, more manoeuvrability and portability, and a higher payload to robot weight ratio [13]. The most popular types of sensors are piezoelectric and strain gauges [30]. The RFM for a single connection is described in Figure 1, by Hu, Mann and Gosine [14].



(a) Model of a single link RFM in theoretical

(b) Model of a single link RFM in experimental

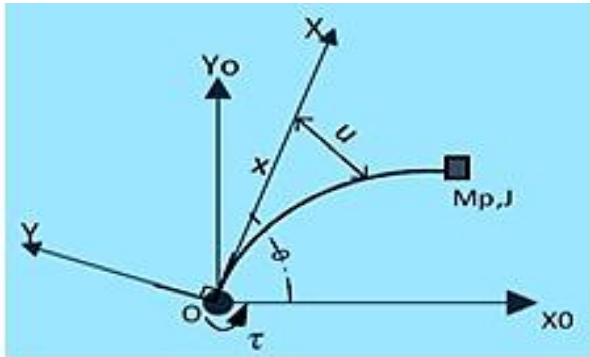
**Fig. 1.** Configurations of a typical RFM (a) Previous studies [13] and (b) [14]

## 2. Methodology

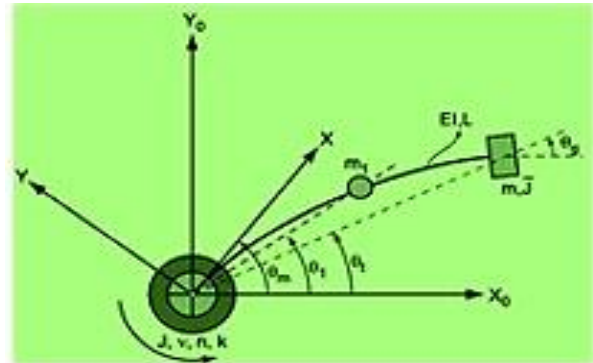
### 2.1 Modelling of Flexible Manipulator (FM) as Main Plant

Here, for the purpose of the performance assessment of the Combined Plant (CP), controller design and simulations, the dynamics, and mathematical modelling for a typical combined single link Robotics Flexible Manipulator (RFM) model as the system main plant is analysed and reviewed

in which it is an arm with moment of inertia ( $I_b$ ), centre of inertia ( $I_h$ ), linear density ( $\rho$ ) and length ( $L$ ) as shown in Figure 2. The main plant model is divided into two sub models, one of which describes the behaviour of the FM while the second describes the behaviour of the DC Servo Motor (DCSM) model as the shaker of main plant.



(a) Typical single link robotics FM



(b) Typical single link robotics FM derivatives

**Fig. 2.** Typical single link robotics FM (a) and its derivatives (b) [15]

In Figure 2, the mass of the load ( $M_p$ ) and the inertia associated with the load ( $I_p$ ) are shown. The control torque  $T(t)$  of the manipulator is applied to the centre of the dc servo motor. The manipulator angular displacement in the ( $X_0OY_0$ ) plane is determined by  $\theta(t)$ . The length of the link is much longer than the width and the link vibration is often in the horizontal direction. Deformation and rotational inertia have been ignored. For ( $\theta$ ) as the displacement angle and ( $u$ ) as the elastic deviation, the sum of the net displacement of a point on the manipulator  $y(x,t)$  in  $X$  distance from the centre which is described as a function in both movements. A hard body movement  $\theta(t)$  and another elastic deviation  $u(x,t)$  in the distance which will be measured by the line  $OX$  is as follows:

$$y(x,t) = x\theta(t) + u(x,t) \quad (1)$$

To get the equations of motion for the manipulator, the related and corresponding energies are calculated. The energies related to the system include kinetic energy, potential, and losses, where in calculations the effect of rotational inertia is ignored. The system kinetic energy has been given as follows:

$$E_k = \frac{1}{2} I_h \dot{\theta}^2 + \frac{1}{2} \int_0^1 \left( \frac{\partial u}{\partial t} + X\dot{\theta} \right)^2 \rho dx + \frac{1}{2} M_p \left( \frac{\partial u}{\partial t} + X\dot{\theta} \right)^2, \quad x=L \quad (2)$$

With the aforementioned equation in mind, the first component on the right is caused by the hub's inertia, the second part is caused by the manipulator's rotation around the hub, and the third part is caused by the load's mass (payload mass), which has been thought to be helpful. The angular velocity and elastic deflection are seen as being modest in this context. Manipulator flexion is connected to potential energy. The consequences of the shear displacement are ignored because the intended link's length is much longer than its thickness. As a result, the system potential energy is as follows:

$$E_p = \frac{1}{2} EI \int_0^1 \left[ \frac{\partial^2 u}{\partial x^2} \right]^2 dx \quad (3)$$

In the above equation, (E) and (I) are the modulus of Young's due to the link and inertia moment features related to its cross-sectional area. Note that, in general, the manipulator movement is in the vertical plane, such as the deformation elastic due to gravitational forces in the vertical direction are both ignored and the flexibility in the vertical direction is minimal. When part of the energy absorbed by the manipulator during its movement is the resistance to the transverse speed given by D(X), the angular speed resistance at the centre by (D<sub>0</sub>) and the strain speed resistance by (D<sub>s</sub>) are expressed. Hence, the energy lost by oscillations and forces has been given as follows:

$$E_F = \frac{1}{2} \int_0^1 D(X) \left( \frac{\partial u}{\partial t} \right)^2 dx + \frac{1}{2} \int_0^1 D_s I \left( \frac{\partial^3 u}{\partial x^2 \partial t} \right)^2 dx + \frac{1}{2} D_0 \left( \frac{\partial^2 u}{\partial x \partial t} \right)^2, \quad x=0 \quad (4)$$

in the dynamic equations of the manipulator movement the work done for the input torque T(t) has been given as following:

$$w = T \theta(t) \quad (5)$$

To get the manipulator's motion equations, the generalized Hamiltonian principle was used.

$$\int_{t_1}^{t_2} (\delta L + \delta W) dt = 0 \quad (6)$$

At times (t<sub>1</sub>) to (t<sub>2</sub>) is assumed (δθ) = (δu) = 0 where (t<sub>1</sub>) and (t<sub>2</sub>) are two parameters at which that (E<sub>k</sub> - E<sub>p</sub> = L) and t<sub>1</sub> is less than t<sub>2</sub> and (L) is the system Lagrange. Where (δw) denotes the virtual work, (δθ) denotes the virtual rotation and (δu) denotes the virtual elastic displacement, hence the Eq. (2), Eq. (3), Eq. (5), have been given as follows:

$$\delta \int_{t_2}^{t_1} [E_k - E_p + W] dt = 0 \quad (7)$$

At high modes and frequencies, the rotation inertia and the shear deformation are more evident and effective. Since this study has demonstrated that the first two modes are enough for manipulator modelling. As a result, the effects of shear deformation and rotational inertia may be disregarded. The above equation is modified to get the manipulator motion equation, which is written as follows:

$$EI \frac{\partial^4 u(x,t)}{\partial x^4} + \rho \frac{\partial^2 u(x,t)}{\partial t^2} = - \rho x \ddot{\theta} \quad (8)$$

by substituting the u(x,t) from Eq. (2) into Eq. (7) the manipulator motion equation according to y(x,t) is expressed as follows:

$$EI \frac{\partial^4 y(x, t)}{\partial x^4} + \rho \frac{\partial^2 y(x, t)}{\partial t^2} = 0 \quad (9)$$

The above equation is a quadratic partial differential equation. This relationship shows the equation dynamically describing the flexible manipulator motions while considering a wide mass. This mass has torque because it is decentralized but the mass ( $m_1$ ) has no torque because it is centralized and focused. Considering the boundary conditions of the system, the dynamic conditions, and the investigation of the dynamic equilibrium of the system as well as the geometrical relationships governing the system Hence, the state space equation for the dynamics of the system has been given as follows:

$$\dot{X}(t) = Ax(t) + Bu(t) \quad (10)$$

$$\dot{Y}(t) = Cx(t) + Du(t) \quad (11)$$

$$\dot{X}_s = [A] X_s + [B] \theta_m, \quad \dot{X}_s = [C] X_s + [D] \theta_m \quad (12)$$

$$A = \begin{bmatrix} 0 & 0 & 0 & 1 & 0 & 0; & 0 & 0 & 0 & 0 & 1 & 0; & 0 & 0 & 0 & 0 & 1; & -192\delta & 192\delta & -48\delta & 0 & 0 & 0; & 48\rho & -60\rho & 18\rho & 0 & 0 & 0; & -12\gamma & 18\gamma & -7\gamma & 0 & 0 & 0 \end{bmatrix} \quad (13)$$

$$B = \begin{bmatrix} 0; & 0; & 0; & 48 & \delta & ; & -6 & \rho & ; & \gamma \end{bmatrix} \quad (14)$$

$$C = \begin{bmatrix} 1 & 0 & 0 & 0 & 0 & 0; & 0 & 1 & 0 & 0 & 0 & 0; & 0 & 0 & 1 & 0 & 0 & 0 \end{bmatrix} \quad (15)$$

$$D = \begin{bmatrix} 0; & 0; & 0 \end{bmatrix} \quad (16)$$

where the state variables are as  $X_s^T = [\theta_1, \theta_t, \theta_g, \dot{\theta}_1, \dot{\theta}_t, \dot{\theta}_g]$  and the constants used for simplifying the matrix shape are as ( $\gamma = \frac{EI}{JL}$ ), ( $\rho = \frac{EI}{M_p L * L * L}$ ) and ( $\delta = \frac{EI}{M_1 L}$ ). Hence, the system transfer function of the output to input has been given as follows:

$$\frac{\theta_1(s)}{\theta_m(s)} = \frac{48 \delta (s^4 + (6\gamma + 36\rho)s^2 + 48\gamma\rho)}{s^6 + (7\gamma + 60\rho + 192\delta)s^4 + (96\gamma\rho + 768\gamma\delta + 2304\rho\delta)s^2 + 2304\gamma\rho\delta} = \frac{K1}{\Delta} \quad (17)$$

$$\frac{\theta_t(s)}{\theta_m(s)} = \frac{-6\rho (s^4 + (4\gamma - 192\delta)s^2 - 384\delta\gamma)}{s^6 + (7\gamma + 60\rho + 192\delta)s^4 + (96\gamma\rho + 768\gamma\delta + 2304\rho\delta)s^2 + 2304\gamma\rho\delta} = \frac{K2}{\Delta} \quad (18)$$

$$\frac{\theta_g(s)}{\theta_m(s)} = \frac{\gamma (s^4 - (48\rho + 384\delta)s^2 + 2304\rho)}{s^6 + (7\gamma + 60\rho + 192\delta)s^4 + (96\gamma\rho + 768\gamma\delta + 2304\rho\delta)s^2 + 2304\gamma\rho\delta} = \frac{K3}{\Delta} \quad (19)$$

## 2.2 Modelling of Gyroscope (G) as Main Actuator

This section looks at one of the most fascinating areas of rotational dynamics, which is the study of rotating solid objects like gyroscopes (G), tops, hoops, and wheels. Gyroscopes have a wide range of uses in engineering navigation and control systems and offer a number of benefits. They have been used for a long time to regulate the attitude of satellites, ships, vehicles, robots, and even humans. The primary function of the gyroscope is to maintain the rotor's axis, and the mathematical model that describes this function is based on the conservation of kinetic energy and variations in angular momentum. Figure 3 depicts the analysis, dynamics, and mathematical modelling for a typical gyroscopic and the motion examined using the Euler Angles ( $\phi$ ), ( $\theta$ ), and ( $\psi$ ). This section develops the equations that describe the motion of a body (top) revolving around a fixed point and being symmetrical with respect to an axis. These equations are used to model the motion of a gyroscope-specific device [17-20]. Precession occurs when a flywheel is rotating about its ( $\omega$ ) axis and an external disturbance is applied around its ( $\theta$ ) axis. If the flywheel has enough angular momentum, it will remain horizontal and start to spin along its ( $\alpha$ ) axis which this precession is seen in Figure 4.

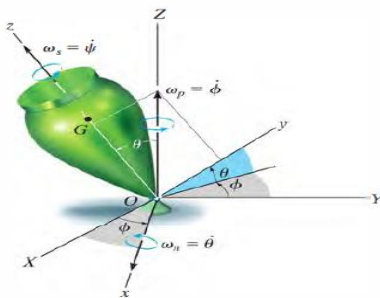


**Fig. 3.** Typical gyroscope angles and motion [16]

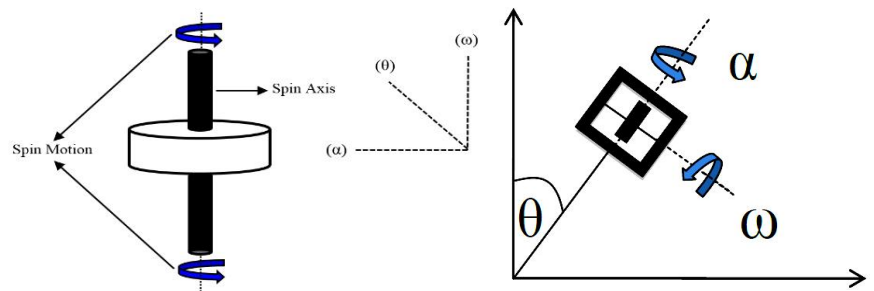


**Fig. 4.** Typical gyroscope as an actuator and precession phenomenon

In this study the states of the gyroscopic motion have been considered with the assumptions of Euler angles ( $\phi$ ), ( $\theta$ ), ( $\psi$ ) and their derivatives as below models shown in Table 1. where the ( $w_p = \dot{\phi}$ ) is the angular velocity of precession around the z axis in radians/second, ( $w_n = \dot{\theta}$ ) is the angular velocity of nutation in radians/second and ( $w_s = \dot{\psi}$ ) is the angular velocity of the wheel (rotor) which is called the spin velocity around the symmetrical axis in radians/second. Here the ( $\ddot{\phi}$ ), ( $\ddot{\theta}$ ) and ( $\ddot{\psi}$ ) are as angular accelerations and ( $T_x = M_x$ ), ( $T_y = M_y$ ) and ( $T_z = M_z$ ) are as torques. ( $L$ ) is the rod length ( $r$ ) being the rotor radius and ( $\theta$ ) is the angle between the rod and ( $z$ ) vertical axis which is a constant. As the rotor spins at a constant rate ( $w_s$ ), the gyroscopic actuator processes at a constant rate ( $w_p$ ) about the pivot at the base with ( $\theta$ ) constant but in this research study it is fixed at the fixed point without any rotation. Starting with the ( $X$ ), ( $Y$ ), ( $Z$ ) and ( $x$ ), ( $y$ ), ( $Z$ ) axes in coincidence Figure 3, the final position of the top, the angular velocity components ( $\dot{\phi}$ ), ( $\dot{\theta}$ ) and ( $\dot{\psi}$ ) are known as the precession, nutation and spin respectively therefore the angular velocity ( $w$ ) of the gyroscope actuator can be determined and has been given as following:

**Table 1**

States of gyroscope motion with assumptions of the Euler angles

Definitions	State 1	State 2
Phi Angle - ( $\phi$ )	variable	constant
Theta Angle - ( $\theta$ )	variable	constant

Psi Angle - ( $\psi$ )	variable	constant
Angular Velocity – Precession ( $\dot{\phi}$ )	variable	0
Angular Velocity - Nutation - ( $\dot{\theta}$ )	variable	0
Angular Velocity - Spin - ( $\dot{\psi}$ )	variable	0
Angular Acceleration - ( $\ddot{\phi}$ )	variable	0
Angular Acceleration - ( $\ddot{\theta}$ )	variable	0
Angular Acceleration - ( $\ddot{\psi}$ )	variable	0
Torque - ( $T_x$ )	variable	0
Torque - ( $T_y$ )	variable	0
Torque - ( $T_z$ )	variable	0
Torque - ( $T_T$ )	variable	0

$$w = w_x i + w_y j + w_z k = \dot{\theta} i + (\dot{\phi} \sin\theta) j + (\dot{\phi} \cos\theta + \dot{\psi}) k \quad (20)$$

and the angular velocity ( $\Omega$ ) of the axis has been given as following:

$$\Omega = \Omega_x i + \Omega_y j + \Omega_z k = \dot{\theta} i + (\dot{\phi} \sin\theta) j + (\dot{\phi} \cos\theta) k \quad (21)$$

The (x), (y) and (z) reference's motion affects the three scalar equations of rotational motion. These axes are frequently positioned to be the main axis of inertia. The equations are known as the Euler equations of motion if the axes are fixed in and move with the body as shown by (w). The following equations result from the motion of the gyroscopic actuator taken into account as indicated above:

$$w \neq \Omega, \quad w_x = \dot{\theta} = w_n, \quad w_y = \dot{\phi} = w_p, \quad w_z = \dot{\psi} = w_s, \quad I_x = I = 0.5, \quad I_z = 0.1 \quad (22)$$

and the gyroscope equations of motion are as the following:

$$\sum M_x = I_x \dot{w}_x - I_y \Omega_z w_y + I_z \Omega_y w_z = I_x \ddot{\theta} - I_y \Omega_z \dot{\phi} + I_z \Omega_y \dot{\psi} \quad (23)$$

$$\sum M_y = I_y \dot{w}_y - I_z \Omega_x w_z + I_x \Omega_z w_x = I_y \ddot{\phi} - I_z \Omega_x \dot{\psi} + I_x \Omega_z \dot{\theta} \quad (24)$$

$$\sum M_z = I_z \dot{w}_z - I_x \Omega_y w_x + I_y \Omega_x w_y = I_z \ddot{\psi} - I_x \Omega_y \dot{\theta} + I_y \Omega_x \dot{\phi} \quad (25)$$

in this research study the dynamics and mathematical model as Table 1 of the gyroscope with the state variables is considered shown and determined in state space as following:

$$x_1 = \phi, \quad x_2 = \theta, \quad x_3 = \psi, \quad x_4 = \dot{\phi}, \quad x_5 = \dot{\theta}, \quad x_6 = \dot{\psi} \quad (26)$$

which (x) is the state variable. The state space equations of the gyroscope are expressed as following:

$$T_x = \sum M_x = I_x \ddot{x}_2 - I_y \Omega_z \dot{x}_1 + I_z \Omega_y \dot{x}_3 \quad (27)$$

$$T_y = \sum M_y = I_y \ddot{x}_1 - I_z \Omega_x \dot{x}_3 + I_x \Omega_z \dot{x}_2 \quad (28)$$

$$T_z = \sum M_z = I_z \ddot{x}_3 - I_x \Omega_y \dot{x}_2 + I_y \Omega_x \dot{x}_1 \quad (29)$$

The relation between state space equations of the gyroscope actuator motion and state variables is expressed as the following:

$$\dot{X}_1 = \dot{\phi} = X_4, \quad \dot{X}_2 = \dot{\theta} = X_5, \quad \dot{X}_3 = \dot{\psi} = X_6 \quad (30)$$

$$\dot{X}_4 = T_y/I_y + I_z/I_y \Omega_x \dot{\psi} - I_x/I_y \Omega_z \dot{\theta} \quad (31)$$

$$\dot{X}_5 = T_x/I_x + I_y/I_x \Omega_z \dot{\phi} - I_z/I_x \Omega_y \dot{\psi} \quad (32)$$

$$\dot{X}_6 = T_z/I_z + I_x/I_z \Omega_y \dot{\theta} - I_y/I_z \Omega_x \dot{\phi} \quad (33)$$

$$\dot{X} \quad (t) = Ax(t) + Bu(t) \quad (34)$$

$$\dot{Y} \quad (t) = Cx(t) + Du(t) \quad (35)$$

which ( $I_x$ ), ( $I_y$ ) and ( $I_z$ ) are the moments of inertia which are represented the moments and products of inertia which is determined by direct integration by using tabulated values. This is a nice compact and total equation which is solve for any of the values ( $\phi$ ), ( $\theta$ ), ( $\psi$ ), ( $w_p$ ), ( $w_n$ ) and ( $w_s$ ) if the other two values are known. If the mass of the rod is negligible then ( $m_r = I_r = I_{py} = 0$ ) and the above equation simplifies to a general equation for uniform gyroscope actuator motion with negligible rod mass. In this study the state of the gyroscope actuator motion has been considered as the rotation of the rotor at a fixed-point state with the assumptions of below states and model shown in Table 2 which ( $\dot{\phi}$ ) must be a constant as that is not the target for control ( $\dot{\psi}$ ) must be a variable as the target control therefore ( $\psi$ ) must be a variable and ( $\ddot{\psi}$ ) must be a variable. Due to the state of the gyroscope motion as considered and mentioned above in Table 2 the gyroscope equations of motion are developed as the following:

Gyroscope equations of motion in model as Table 2.

$$T_x = \sum M_x = 0 \quad (36)$$

$$T_y = \sum M_y = 0 \quad (37)$$

$$T_z = \sum M_x = I_x \ddot{\psi} + I_z \ddot{\phi} \cos\theta - I_z \dot{\phi} \dot{\theta} \sin\theta \quad (38)$$

Considering the dynamics and mathematical model in Table 2 of the gyroscope with the state variables (x) is shown and determined in state space and equations of the gyroscope is expressed as following:

Gyroscope equations of motion in state space of model as Table 2.

$$T_z = \sum M_x = I_x \ddot{\psi} + I_x \ddot{\phi} \cos\theta - I_x \dot{\phi} \dot{\theta} \sin\theta \quad (39)$$

A closed form solution is typically not possible because the general gyroscope equations of motion are a linked set of nonlinear second order differential equations. Instead, by employing numerical analysis and computer techniques, the Euler angles may be represented visually as functions of time; hence, the special instances have been treated in Table 2 and Table 3.

**Table 2**  
 States of proposed gyroscope motion as rotation of rotor at a fixed point

Definitions	State 3
Phi Angle - ( $\phi$ )	variable
Theta Angle - ( $\theta$ )	constant
Psi Angle - ( $\psi$ )	variable
Angular Velocity - Precession - ( $\dot{\phi}$ )	0
Angular Velocity - Nutation - ( $\dot{\theta}$ )	0
Angular Velocity - Spin - ( $\dot{\psi}$ )	variable
Angular Acceleration - ( $\ddot{\phi}$ )	0
Angular Acceleration - ( $\ddot{\theta}$ )	0
Angular Acceleration - ( $\ddot{\psi}$ )	variable
Torque - ( $T_x$ )	0
Torque - ( $T_y$ )	0
Torque - ( $T_z$ )	variable
Torque - ( $T_t$ )	variable
For State 3: $T_t = T_z$ , $T_x = T_y = 0$	

**Table 3**  
 Technical specification of gyroscope

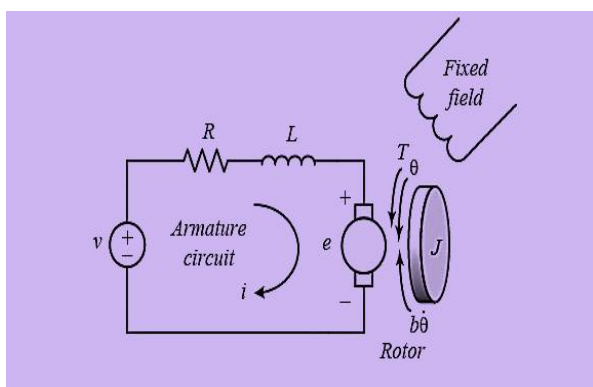
Para.	Rate	Title	Unit
$I_{arm}$	0.89	Moment of the	(kg/m <sup>2</sup> )
$M_g$	5.9	Mass of gyro	(kg)
$M_f$	2.9	Mass of flywheel	(kg)
$M_a$	3.87	Mass of arm	(kg)
R	0.083	Distance to centre of flywheel	(m)
r	0.0605	Radius of flywheel	(m)
$H_{cg}$	0.22	Height of arm centre of gravity	(m)

w	10000	Flywheel speed	(rad/s)
	*		
	$\pi/(180*60)$		

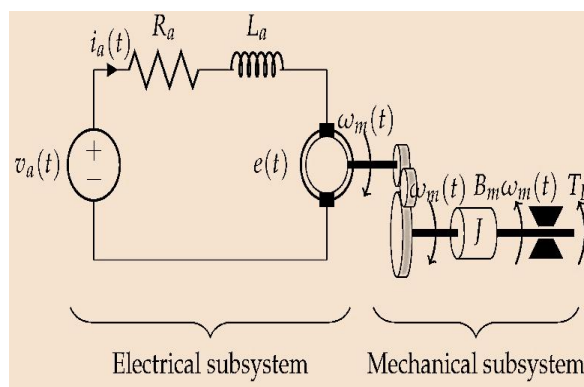
### 2.3 Modelling of DCSM as FM Shaker and DCM as Gyroscope Driver

An energy converter, the motor transforms electrical energy from the source into mechanical energy for the load. The majority of mechanical demands can be accommodated by the torque and speed characteristics of motors. As a result, motors provide excellent platforms for sophisticated control algorithms. These motors' excellent controllability has led to their widespread application, therefore controlling their speed is necessary. Supply voltage, armature resistance, and the field flux created by the field current all affect the motor's position and speed. Armature voltage control, armature resistance control, and field flux control are the techniques used to regulate the position and speed of these motors. This study uses MATLAB & SIMULINK to analyse motor performance utilizing mathematical expression, time domain, and frequency domain approaches.

$$T = K_t \quad (40)$$



(a) Typical DC motor with armature circuit



(b) Free body diagram

**Fig. 5.** Typical DC motor with armature circuit (a) and free body diagram (b) [21]

$$e = K_e \dot{\theta} = K_e \omega \quad (41)$$

which (V) is the input armature voltage. The motor is analysed by either state space model or Laplace transform. In this paper it is discussed about the dynamic model of motor by Laplace transform equations. With the increase in motor torque ( $\tau$ ), the armature current (i) and increases by an armature constant ( $K_t$ ). With the increase in motor back (e), the rotational and angular velocity ( $\theta = \omega$ ), increases by a motor constant ( $K_e$ ). By combination of newton's law with Kirchhoff's law from Figure 4 the equations are as following:

$$J \ddot{\theta} + b \dot{\theta} = K_t i \quad (42)$$

$$L \frac{di}{dt} + R_i i = V - K_e \dot{\theta} = V - K_e \omega \quad (43)$$

where (J) denotes moment of inertia, (b) denotes friction coefficient, (L) denotes armature inductance, (R) denotes armature resistance, (V) denotes input voltage, (K) denotes electromotive force constant, and ( $\theta$ ) denotes angular acceleration. In state space, the output is angular velocity, while the inputs are voltage (V) and the rotation speed and current. The following are the equations for motor analysis using the Laplace transform:

$$Js^2 \theta(s) + bs \theta(s) = K \int I(s) \quad (44)$$

$$Ls \omega(s) + R I(s) = V(s) - K_s \theta(s) \quad (45)$$

$$Js^2 \theta(s) + bs \theta(s) = K \left( \frac{[V(s) - K_s \theta(s)]}{R + sL} \right) = K \frac{[V(s) - K_s \theta(s)]}{R + sL} \quad (46)$$

in this research paper this motor with an ideal train gear is proposed and considered as an auxiliary in shaker and driver for the CP and NGCAM in the intelligent control framework as shown in Table 4 and Table 5.

**Table 4**  
 Technical specification of DCSM

Parameters	Rate	Title	Unit
K = K <sub>b</sub> = K <sub>t</sub>	7.67E-3	Electromotive force constant	(N*m/A)
R	2.6	Electrical resistance	(Ω)
L	180	Electrical inductance	(μH)
J	5.3E-7	Moment of inertia of the rotor	(kg*m <sup>2</sup> )
D=B	7.7E-6	Damping ratio	(Nms)
K = K <sub>b</sub> = K <sub>t</sub>	7.67E-3	Electromotive force constant	(N*m/A)
R	2.6	Electrical resistance	(Ω)
L	180	Electrical inductance	(μH)
J	5.3E-7	Moment of inertia of the rotor	(kg*m <sup>2</sup> )
D=B	7.7E-6	Damping ratio	(Nms)

**Table 5**  
 Technical specification of DCM

Parameters	Rate	Title	Unit
K = K <sub>e</sub> = K <sub>t</sub>	0.01	Electromotive force constant	(Nm/Amp)
R	1	Electrical resistance	(Ω)
L	0.5	Electrical inductance	(H)
J	0.01	Moment of inertia of the rotor	(kg.m <sup>2</sup> / s <sup>2</sup> )
B	0.1	Damping ratio	(Nms)

#### 2.4 Modelling of Combined Plant (CP)

Here, the Combined Plant (CP) model consists of a robotics flexible manipulator model as the main plant and a direct current servo motor model as an auxiliary actuator and shaker has been considered which the input and output is the angular position. The Linearization at model initial condition with continuous-time transfer function with output/input ( $O_1/I_1$ ) as angular position as following and the time and frequency responses of CP transfer function.

$$-1219 s^4 + 4.33e-11 s^3 - 5.385e07 s^2 + 3.408e-07 s + 8.994e10$$

$$s^{10} + 12 s^9 + 9.202e04 s^8 + 1.104e06 s^7 + 2.686e08 s^6 + 3.201e09 s^5 + 5.031e10 s^4 + 5.397e11 s^3 + 9.003e11 s^2 - 3.147e-06 s + 1.152e-34 \quad (47)$$

The time-domain and frequency-domain analysis is essential for comprehending the stability and performance characteristics of CP, according to the modelling and continuous-time transfer function of this (CP) as a tenth order transfer function. The frequency response of CP may be plotted and analysed using the bode and Nyquist responses, as well as the step and impulse responses, which are two more common methods. According to the order of the CP open loop transfer function, Figures 6, the inconsistency in this case is quite obvious.

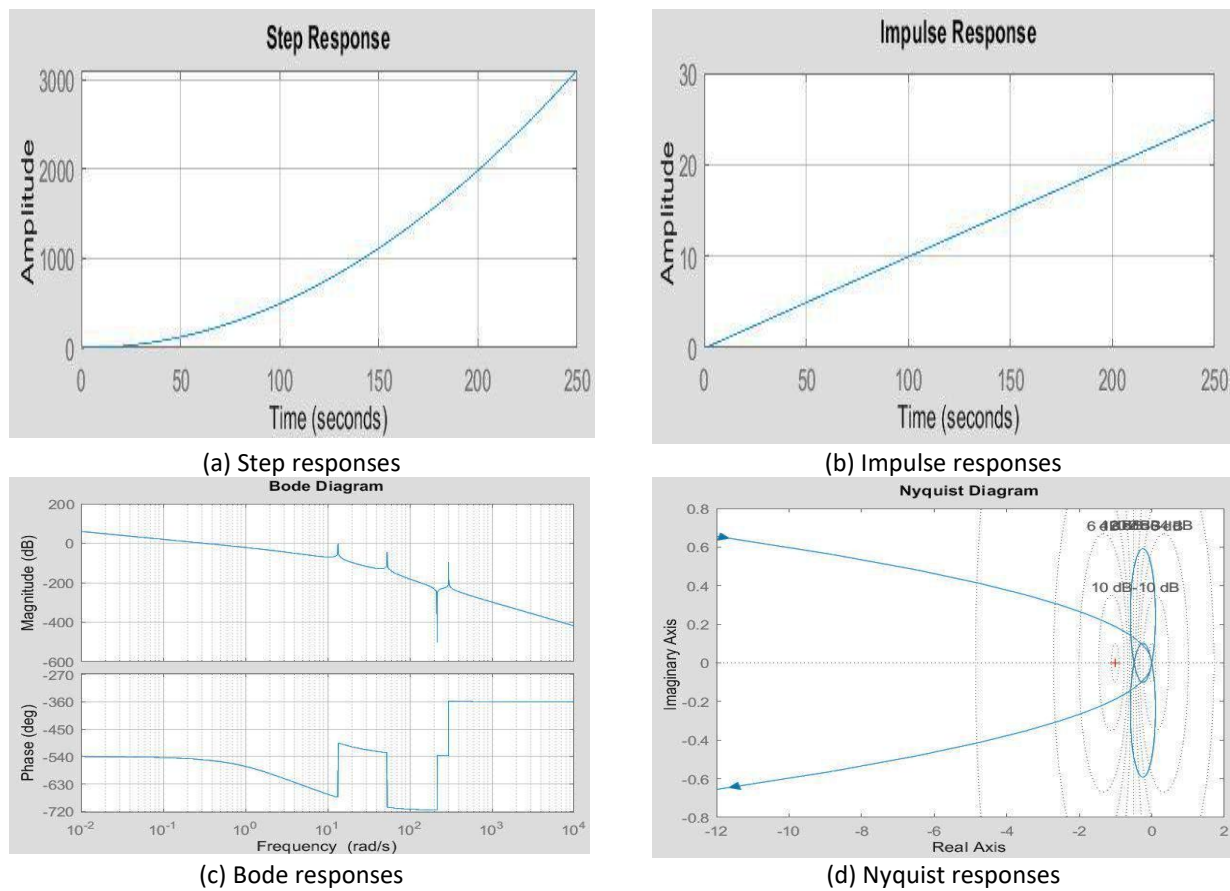


**Fig. 6.** The time-domain (a), (b) and frequency-domain (c), (d) analysis of CP

### 2.5 Modelling of NGCAM as Combined Actuator (CA)

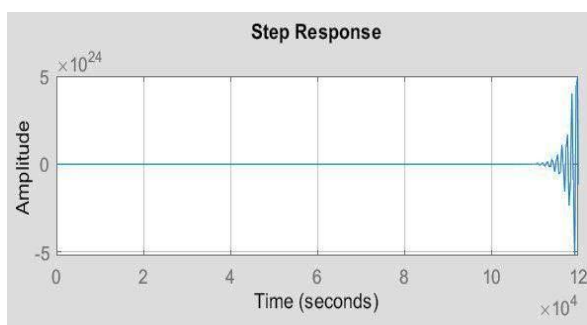
Here, the NGCAM as Combined Actuator (CA) model consists of a gyroscope model as the main actuator and a direct current motor model as the auxiliary actuator and driver has been considered with input/output ( $O_1/I_1$ ) as angular velocity. The NGCAM is divided into two sub models, one of which explains the behaviour of the gyroscope and the other the behaviour of the DCM. In this study the state of the gyroscope motion has been considered as the rotation of the rotor at a fixed-point state with the assumptions of Euler angles ( $\phi$ ), ( $\theta$ ) and ( $\psi$ ) and their derivatives states in PGGM [16,17].

### 2.6 Modelling of Mechatronics Test Rig System (MTRS)

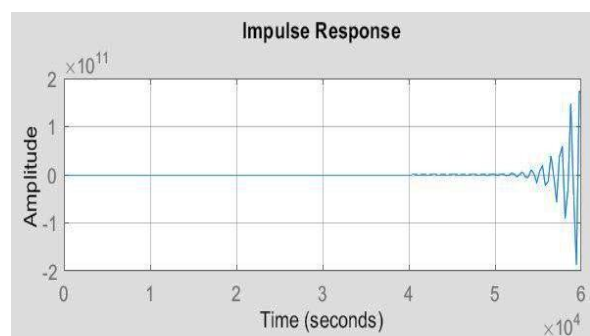
The combination of the Combined Plant (CP) consists of RFM and DCSM and the NGCAM as Combined Actuator (CA) consists of G and DCM has been considered as the MTRS with three degrees of freedoms ( $\theta_1$ ), ( $\theta_t$ ) and ( $\theta_g$ ) which the input and output is the angular position with ( $\theta_t$ ) as the main output of the MTRS. Here, the dynamics and mathematical model of MTRS have been derived using the energy method based on the Lagrange Equation (LE) beam theory, the state space, and the Laplace transform method in the continuous-time domain. As previously mentioned, ( $\theta_m$ ) is the angular position of the output of the motor gearbox and the MTRS has three degrees of freedom ( $\theta_1$ ), ( $\theta_t$ ) and ( $\theta_g$ ). In the dynamical equations of the RFM under investigation in this paper, it is modelled by a flexible beam with a mass in the centre that freely can be bend on the horizontal surface and plane but remains rigid in the vertical axis direction without any rotation. To avoid problems caused by the increase in length at different times, a fixed arm length is assumed in which an arm with a moment of inertia ( $I_b$ ), centre of inertia ( $I_h$ ), linear density ( $\rho$ ) and the length ( $L$ ) has been used. The first step in designing an RFM to improve the performance of a manipulator is to create a relatively realistic dynamic model that takes into account the link's flexibility. The flexible manipulator's mathematical structure is developed from energy concepts by Moloody *et al.*, [22]. The linearization at model initial condition with continuous-time transfer function with input/output ( $O_1/I_1$ ) as angular position as following.

$$\begin{aligned}
 & -1219 s^4 + 8.66e-12 s^3 - 5.385e07 s^2 + 8.994e10 \\
 & \text{-----} \\
 & s^{10} + 12 s^9 + 9.202e04 s^8 + 1.104e06 s^7 + 2.686e08 s^6 + 3.201e09 s^5 + 5.031e10 s^4 + \\
 & 5.397e11 s^3 + 9.003e11 s^2 + 0.07881 s + 0.1378 \qquad \qquad \qquad (48)
 \end{aligned}$$

The time-domain and frequency-domain analysis is crucial for comprehending the stability and performance characteristics of MTRS, according to the modelling and continuous-time transfer function of this (MTRS) as a tenth order transfer function. The frequency response of MTRS may be plotted and analysed using the bode and Nyquist responses, as well as the step and impulse responses, which are two more common methods. In this case, the inconsistency is very obvious when compared to the MTRS open loop transfer function, Figures 7.



(a) Step responses



(b) Impulse responses

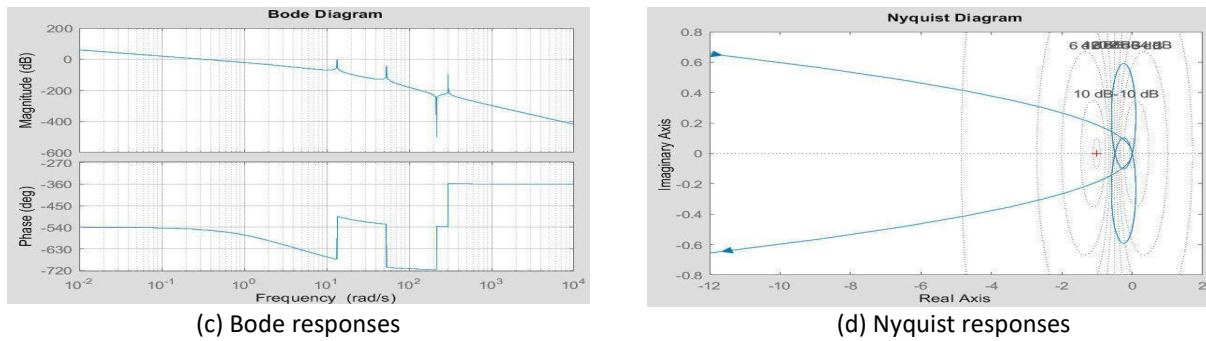
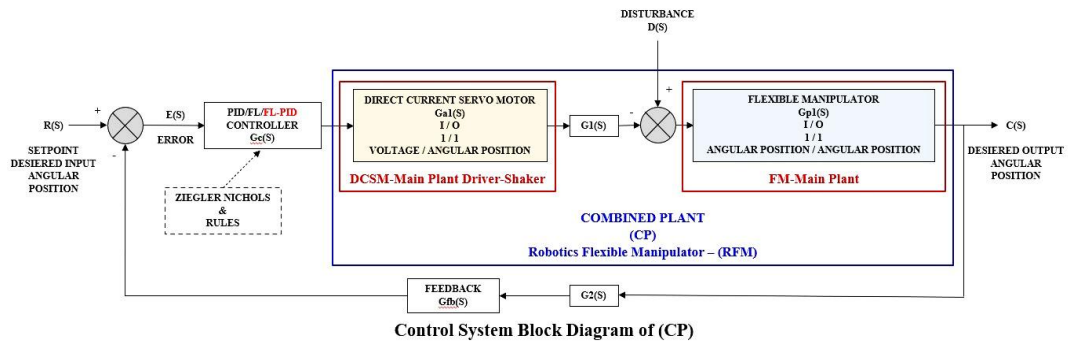


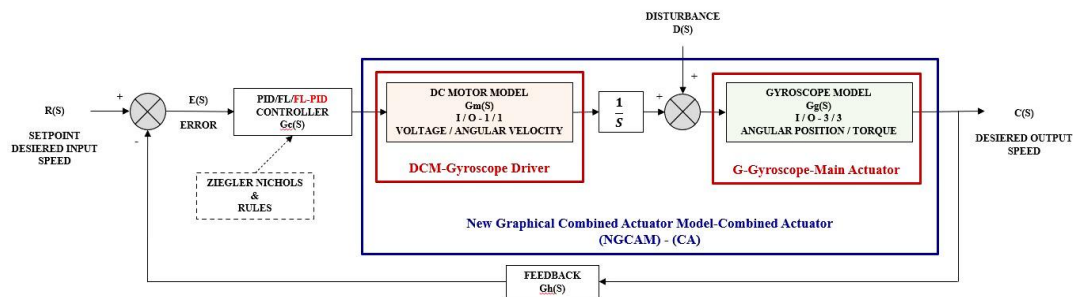
**Fig. 7.** The time-domain (a), (b) and frequency-domain (c), (d) analysis of MTRS

## 2.7 System Controller Development

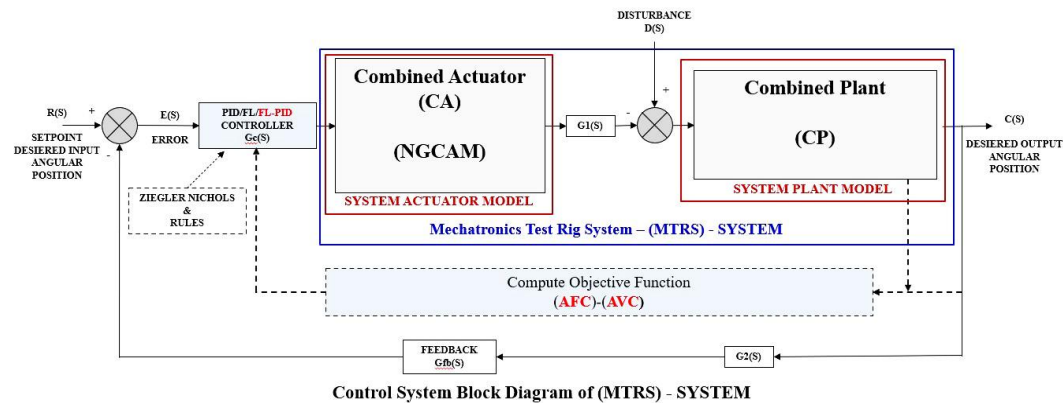
The combination of the Combined Plant (CP) and the NGCAM as the Combined Actuator (CA) has been considered as the system with three degrees of freedoms ( $\theta_1$ ), ( $\theta_t$ ) and ( $\theta_g$ ) which the input and output is the angular position with ( $\theta_t$ ) as the main output of the system. The suggested (AVC-FL-PID) control scheme is employed in this research study to assess system performance in vibration control when the RFM is to be acted with the disturbance. Fuzzy Logic (FL) controllers with various membership function groups are created for the suppression of active vibration of a flexible manipulator. The dual-mode controller is also intended to considerably minimize low amplitude vibration close to equilibrium by combining Fuzzy and PID. Multiple fuzzy controllers are analysed and compared using various membership functions and the distribution density of variable domains. Creating an interface for understanding input/output parameters for fuzzification is the first step in creating a fuzzy controller. By delivering a power signal to the NGCAM actuator through a voltage amplifier, the output value ( $u$ ) activates the beam. The general block control framework of MTRS is shown in Figure 8. A Proportional, Integral and Derivative (PID) is used as the primary controller to regulate the gyroscope. After the controller has analysed the command data and sent the command set to the flywheel motor driver through communication, the traditional and intelligent control framework communicates the flywheel speed command to the controller wirelessly. The flywheel motor receives its energy from the motor driver. the MTRS's traditional and intelligent control scheme, which employs a gyroscopic effect brought on by a combination of a flywheel's angular momentum and a gimbal's rate of tilt. The aforementioned control block can be attached as a NGCAM for the system's vibration control and employed in a new intelligent control framework block. The gyroscopic force acting in the yaw direction is really controlled by the flywheel's tilt motion [23,24].



(a) Control system block diagram of CP



(b) Control system block diagram of CA



(c) Control system block diagram of MTRS

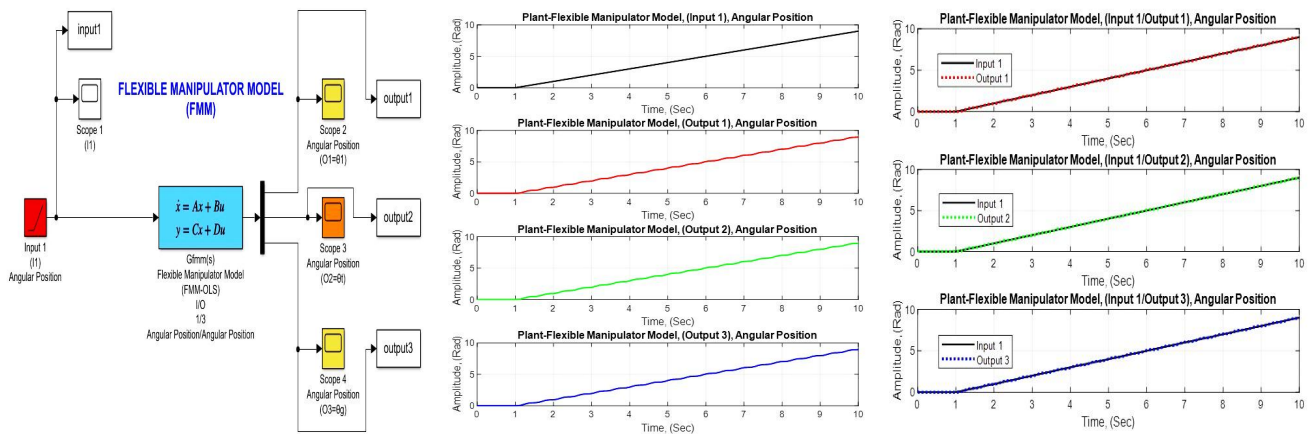
Fig. 8. FL-PID control system block diagram of CP (a), CA (b) and MTRS (c)

### 3. Results

Here, the MATLAB simulations, control strategies, results, and data analysis for the MTRS has been investigated and carried out for the general circuit situation and performance assessment of the MTRS respectively in different models and situations based on mathematical and dynamical modelling, and equations of motion.

#### 3.1 Design and Open Loop State Simulation of FM

Here, the design and open loop state simulation results for a typical single link robotics FM as MTRS main plant has been evaluated in Figure 9.

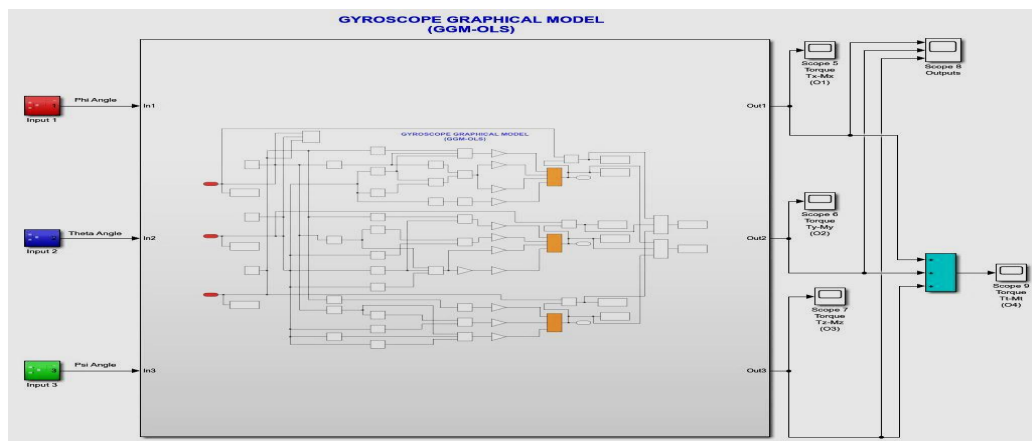


(a) Open loop state simulation of FM (b) Signal graph results of FM (c) Signal graph results of FM  
**Fig. 9.** The open loop state simulation of FM (a) and signal graph results (b) and (c)

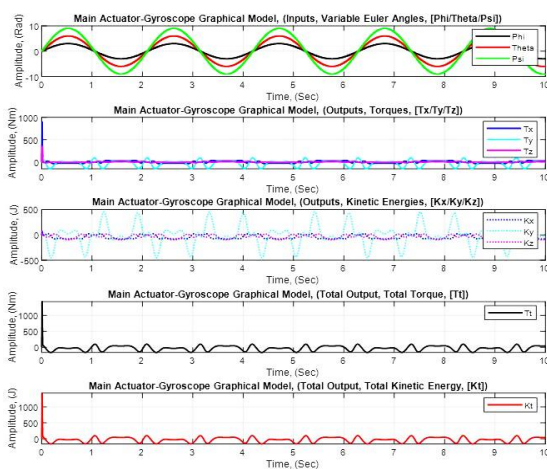
### 3.2 Design and Open Loop State Simulation of G

#### 3.2.1 Gyroscope graphical model (GGM)

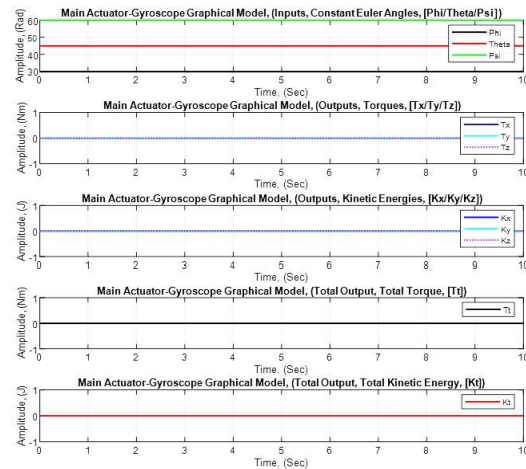
Here, the design and open loop state simulation results for a typical GGM as MTRS actuator has been evaluated in Figure 10.



(a) The control block diagram simulation of GGM



(b) Signal graph results of GGM

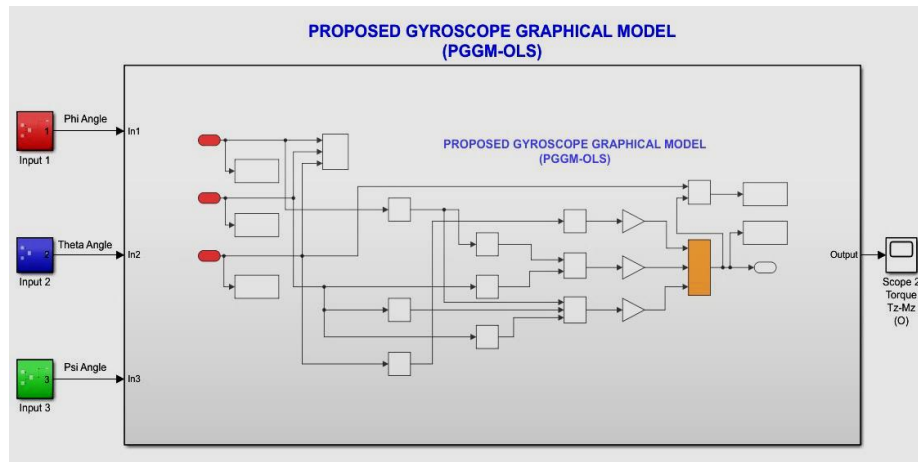


(c) Signal graph results of GGM

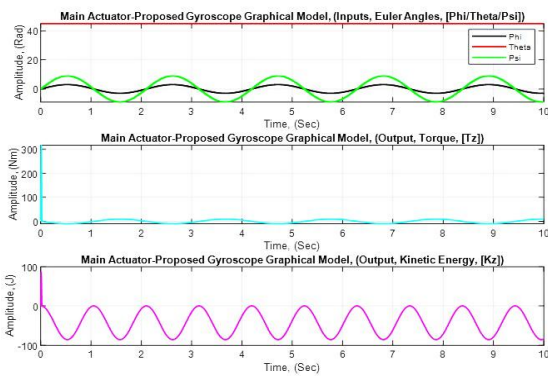
**Fig. 10.** The control block diagram simulation of GGM (a) and the signal graph results (b) and (c)

### 3.2.2 Proposed gyroscope graphical model (PGGM)

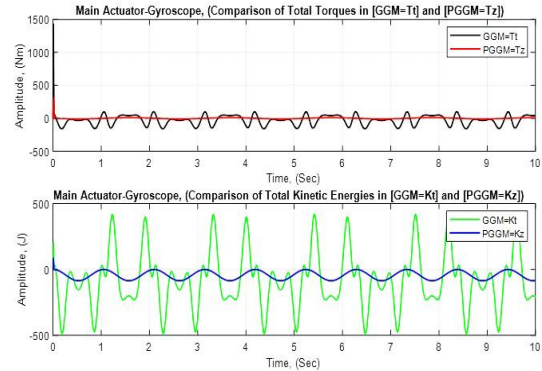
Here, the design and open loop state simulation results for a typical PGGM as MTRS main actuator has been evaluated in Figure 11.



(a) The control block diagram simulation of PGGM



(b) Signal graph results of PGGM

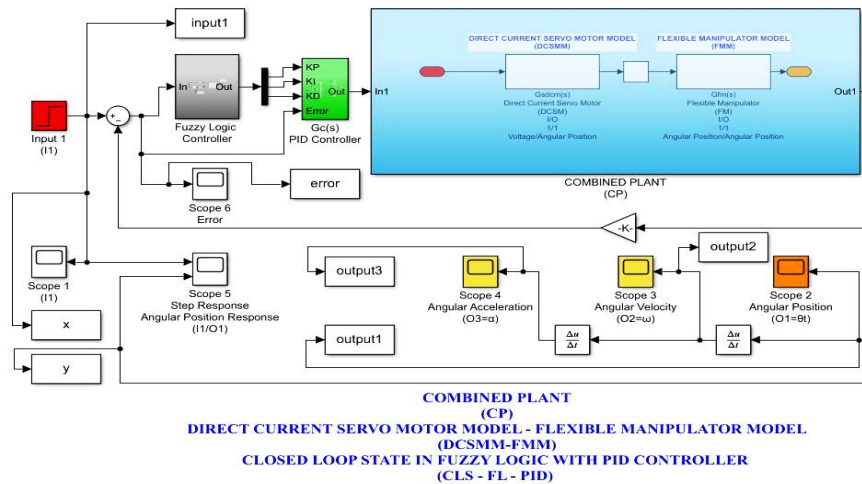


(c) Signal graph results of PGGM

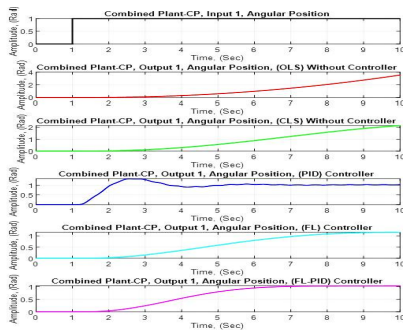
**Fig. 11.** The control block diagram simulation of PGGM (a) and the signal graph results (b) and (c)

### 3.3 Simulation Performance Evaluation of CP

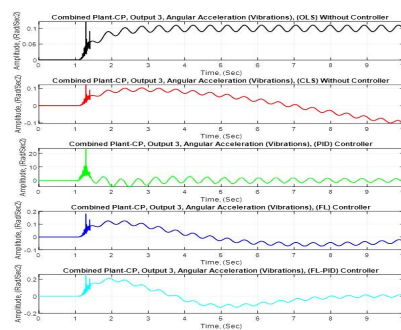
Here, the simulation performance evaluation of CP results has been evaluated in Figure 12 and Table 6.



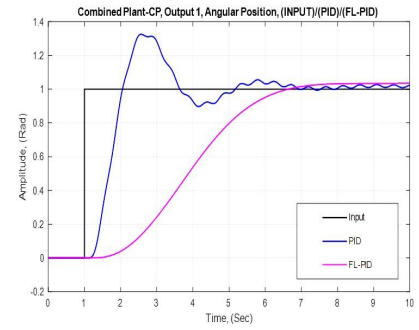
(a) The control block diagram of CP



(b) Angular position signal graph results of CP



(c) Angular acceleration-vibration signal graph results of CP.



(d) Performance evaluation of CP

**Fig. 12.** The control block diagram of CP (a), signal graph results (b), (c) and performance evaluation (d)

**Table 6**  
 Tuned parameters coefficients of PID and FL-PID controller of CP

CP Parameters	PID	FL-PID
$K_p$	0.6986	0.6608
$K_i$	0.6292	0.5952
$K_d$	3.5000	3.2997
N	75.0000	75.0000

5.7 to 5.8 (%) coefficients have been optimized in FL-PID controller.  
 (FL-PID controller is better than PID controller).

### 3.4 Simulation Performance Evaluation of NGCAM

Here, the simulation performance evaluation of NGCAM as CA results has been evaluated in Figure 13 and Table 7.





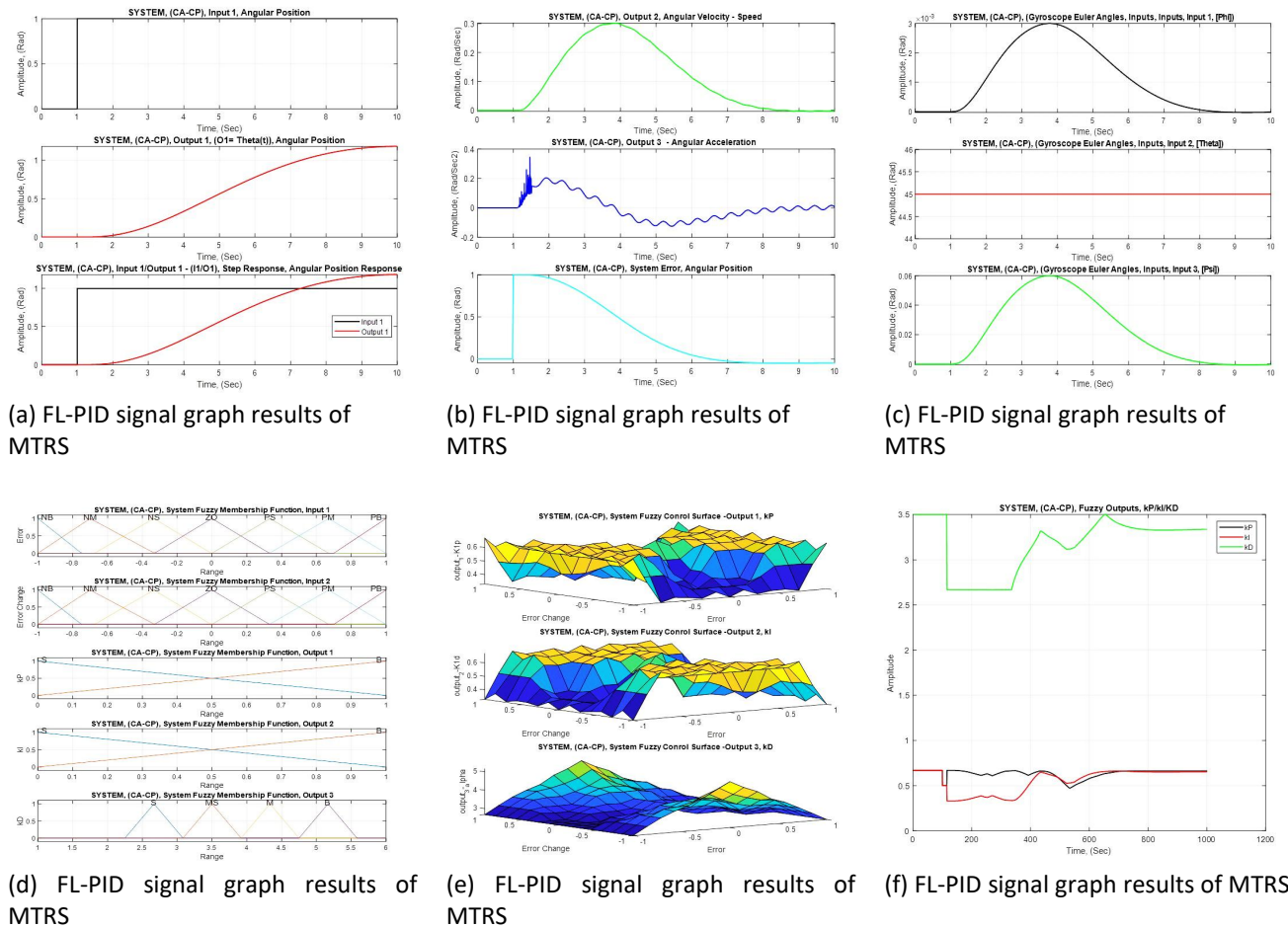
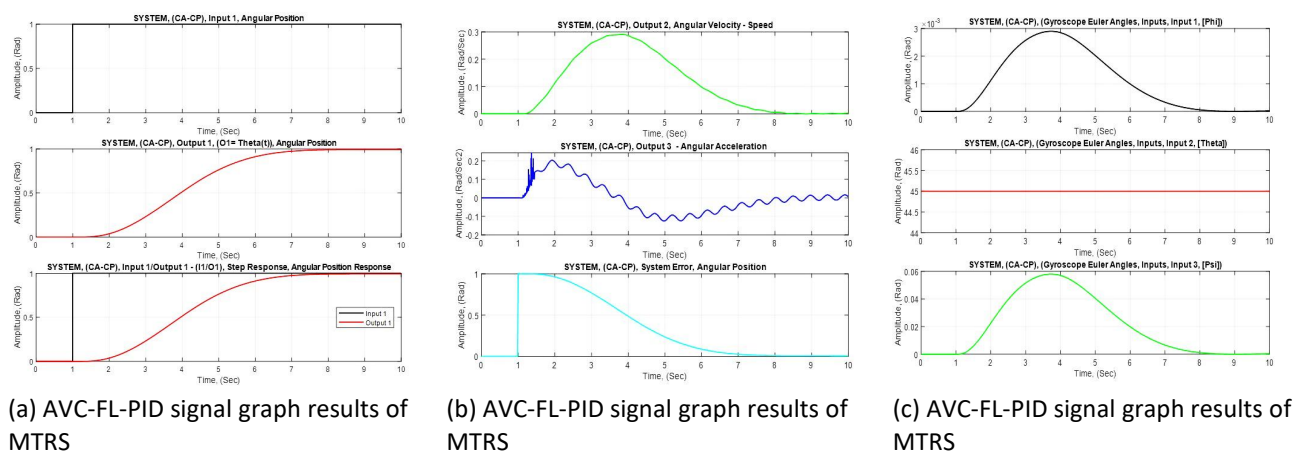
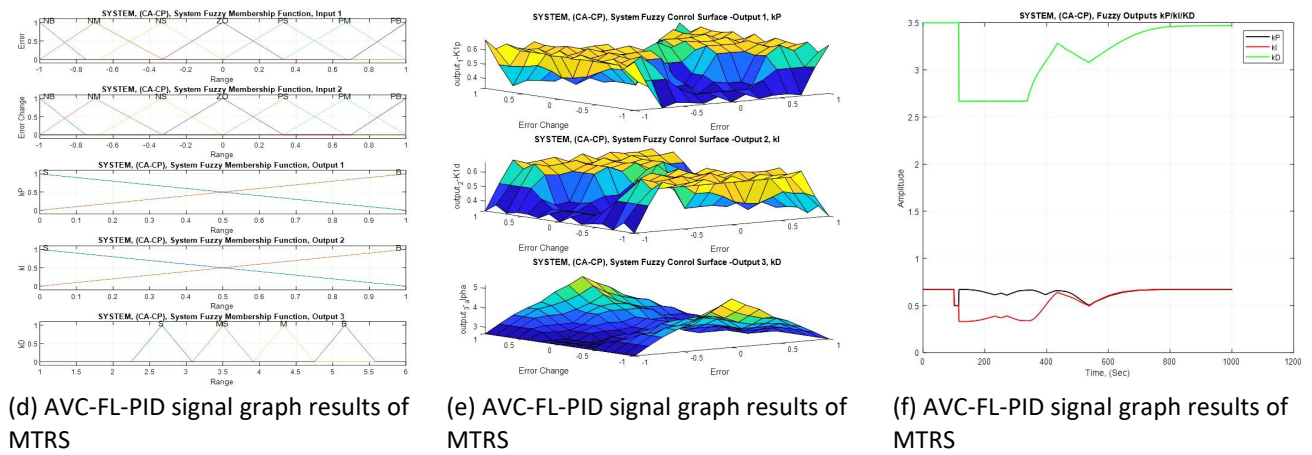


Fig. 16. The FL-PID control simulation of MTRS signal graph results

### 3.5.3 AFC-FL-PID as AVC-FL-PID control simulation of MTRS

Here, the AFC-FL-PID as AVC-FL-PID control simulation of MTRS results has been evaluated in Figure 17.





**Fig. 17.** The AFC-FL-PID as AVC-FL-PID control simulation of MTRS signal graph results

### 3.5.4 Simulation performance evaluation of MTRS

Here, the simulation performance evaluation of MTRS results has been evaluated in Figure 18, Table 8, Table 9, Figure 19, Figure 20 and Figure 21, Figure 22 and Figure 23.

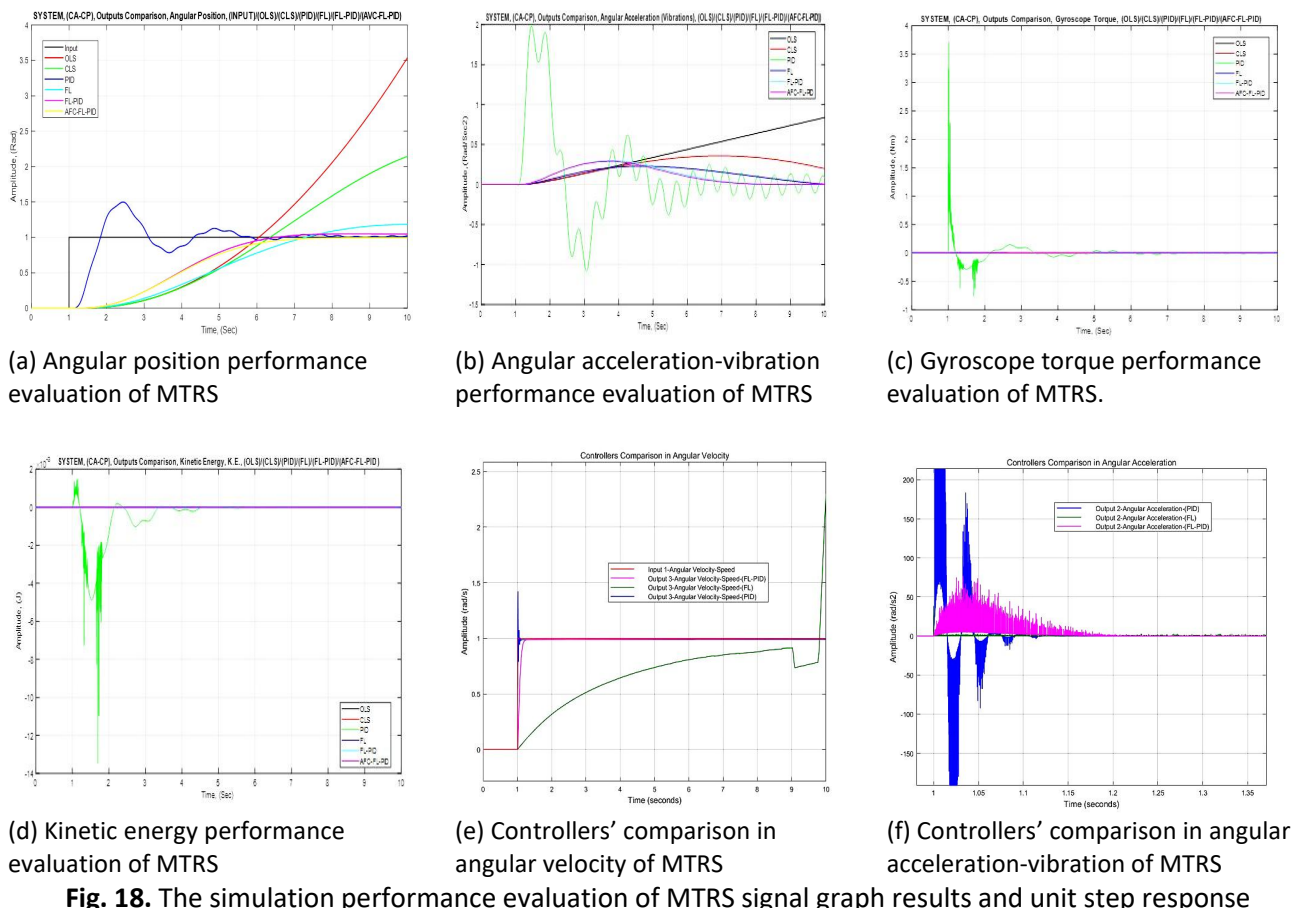


**Fig. 18.** The simulation performance evaluation of MTRS signal graph results and unit step response

**Table 8**

Tuned parameters coefficients of PID, FL and FL-PID controller and performance criteria of MTRS [26-28]

MTRS Parameters	Unit	Description	PID	FL	FL-PID	Reference 1 [26]	Reference 2 [27]	Reference 3 [28]
$K_P$	Cte.	Proportional	0.6744	0.0000	0.6379	0.2033	-	-
$K_I$	Cte.	Integral	0.6051	0.0000	0.5724	0.9333	-	-
$K_D$	Cte.	Derivative	3.3624	0.0000	3.1805	0.0538	-	-
N	Cte.	Cte.	75.0000	0.0000	75.0000	-	-	-
$T_R$	(ms)	Rise Time	1.7546	6.7453	5.3210	-	1.1570	4.0700
$T_P$	(s)	Peak Time	2.5324	9.3210	6.1320	-	1.5000	5.2720
$T_S$	(s)	Settling Time	5.8510	Inf	6.2310	-	2.1850	10.7000
$M_P$	(%)	Overshoot	0.5324	0.1090	0.3993	-	1.5000	0.8190
$E_{SS}$	(/s)	Steady State Error	0.0200	0.1270	0.0140	-	0.0298	0.0982

25 (%)  $M_P$  and 30 (%)  $E_{SS}$  have been optimized as criteria coefficients in FL-PID controller vs PID controller. 27.5 (%) generally is better than comparing to the other systems performance criteria in improvement stabilization and vibration control. (FL-PID controller is a little slow but stable and performance is better than PID controller).

**Table 9**

Tuned parameters coefficients of PID, AVC-PID and AVC-FL-PID controller and performance criteria of MTRS [25,29]

MTRS Parameters	Unit	Description	PID	AVC-PID	AVC-FL-PID	Reference 4 [25]	Reference 5 [29]
$K_P$	Cte.	Proportional	0.6744	0.6796	0.6429	7.1000	4
$K_I$	Cte.	Integral	0.6051	0.6052	0.5725	0.0061	0.03
$K_D$	Cte.	Derivative	3.3624	3.3804	3.1975	70.4600	0.006
N	Cte.	Cte.	75.0000	75.0000	75.0000	-	-
$T_R$	(ms)	Rise Time	1.7546	1.7370	5.0549	-	-
$T_P$	(s)	Peak Time	2.5324	2.4817	5.9254	-	-
$T_S$	(s)	Settling Time	5.8510	5.6754	5.6079	-	-
$M_P$	(%)	Overshoot	0.5324	0.5111	0.3074	-	-
$E_{SS}$	(/s)	Steady State Error	0.0200	0.0198	0.0093	-	-

1 (%) to 5 (%) coefficients have been optimized in AVC-PID controller vs PID controller. 23 (%)  $M_P$  and 33 (%)  $E_{SS}$  have been optimized as criteria coefficients in AVC-FL-PID controller vs PID controller. 28 (%) is so clear and significant optimization is visible than comparing to the other systems in improvement stabilization and vibration control. (AVC-FL-PID controller is better performance than PID controller).

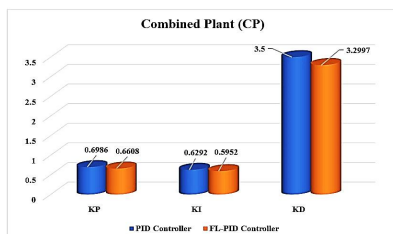


**Fig. 19.** Tuned parameters coefficients of PID and FL-PID controller in CP

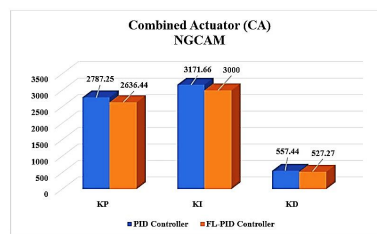


**Fig. 20.** Tuned parameters coefficients of PID and FL-PID controller in CA

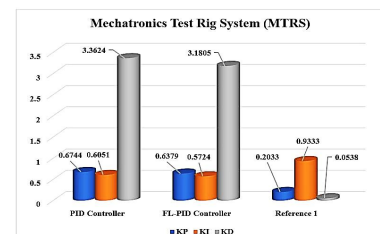


**Fig. 21.** Tuned parameters coefficients of PID, FL-PID controller and reference 1 in MTRS

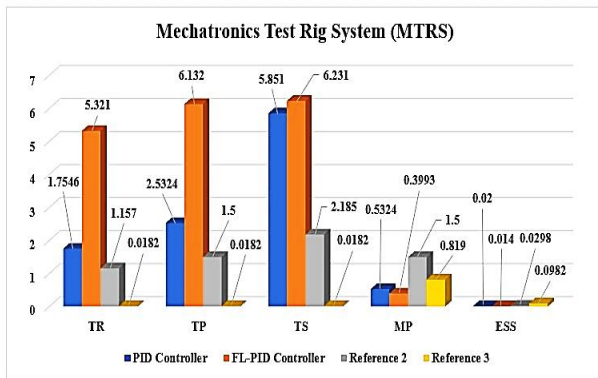


**Fig. 22.** Tuned parameters coefficients of PID, FL-PID controller and references 2 and 3 in MTRS

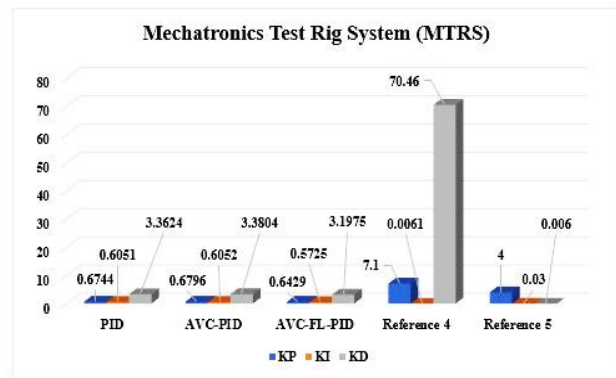


**Fig. 23.** Tuned parameters coefficients of PID, AVC-PID, AVC-FL-PID controller and references 4 and 5 in MTRS

#### 4. Conclusions

There are four types of vibration control systems (VCS): hybrid, semi-active, active, and passive. While some systems are not smart control systems, they are integrated with other smart AVC/SVC systems to create Hybrid Vibration Control (HVC) systems. These systems are actuated by structural motion and require no external force or energy to execute the control. Both the AVC and SVC are intelligent controllable systems that use actuators to gradually change stiffness and damping and produce control forces based on predetermined control algorithms. The AVC system, on the other hand, primarily uses electro-hydraulic or electro-mechanical actuator systems that are self-sufficient in producing control forces with servo-actuator moving mass, necessitating a significant amount of external power. The SVC systems use less electricity than the AVC systems in contrast. Additionally, suitable for combining the flexibility of active devices, which are commonly thought of as controlled passive devices, with the dependability and quality of passive devices. Moreover, HVC systems require the combined use of PVC and AVC/SVC systems. Table 10 provides an overview of the control devices that these control systems use [30].

In this research study from the findings the aim is to control the mechanical vibration of the movement of a CP considered as an RFM and developing a gyroscope device based on a vibrational gyroscope in order to be used in the NGCAM considered as a CA and the control method by AFC-FL-PID considered as AVC-FL-PID. In performance evaluation of Mechatronics Test Rig System (MTRS), it is cleared that in PID control tuned by Ziegler Nichols (ZN) method, the angular position as the output has high ultrasonic and overshoot and have high fluctuations and does not have a proper response which is due to the non-linear elements of the FM in the CP and Gyroscope (G) in the CA. In FL control tuned by fuzzy rules, the angular position as the output is without overshoot and fluctuations but other parameters such as rise time and steady state error are high and in fact the response speed is very slow and has not a good response which is due to the linear elements of DCSM in the CP and DCM in the CA. In FL-PID control as compound controller, the angular position as the output is without overshoot and fluctuations and other parameters such as rise time and steady state error are low and in fact the it is good and very fast in response. As the result the tuned parameters coefficients of PID controller of MTRS have been optimized about 5.7 to 5.8 (%) in FL-PID controller. In AVC-PID, the tuned parameters coefficients of PID controller of MTRS have been optimized about 4.2 to 4.5 (%) and in AVC-FL-PID, more significant optimization is visible. Simulation results illustrate the effectiveness of the proposed strategy which is significantly and quite satisfactory about 25 (%) generally better than comparing to the other systems performance criteria and is so clear and significant optimization is visible than comparing to the other

conventional actuators such as PZTs and other control strategies in improvement stabilization and vibration control of RFM structures. The advantages of the proposed method and the possibilities of further improvements are discussed. Therefore, for a composed of linear and non-linear elements, in order to have better performance it is necessary and suggested to use a combined linear and non-linear controller as here, AVC-FL-PID. The proposed NGCAM model tuned with AVC-FL-PID controller can effectively modifying and producing the simplest control strategy and dynamic equations defining the motion of a gyroscope rotor which is symmetrical with respect to an axis and rotating about a fixed point and is developed which is applied to the motion.

Comparing with the controller criteria coefficients and the performance indicators parameters of the similar systems as references, it is seen that the response and results of the system analysis based on the AVC-FL-PID controller with the NGCAM for the RFM as a new approach are acceptable with a steady state error of 0.35 and quite satisfactory in position and vibration control about 25% better than comparing to the other systems [34-38], in eliminating and minimizing the deflection and oscillation angle of the End Effector of the beam for better performance in improvement stabilization and vibration control of this system and keeping the rotation angle at a certain time in a desired and acceptable positional accuracy in a horizontal plane motion.

**Table 10**  
 Overview of the control devices [30]

No	Passive Energy dissipaters	Passive Isolators	Active	Semi-active	Hybrid
1	Metallic damper	Lead-plug bearing	Active support system	Electrorheological (ER) damper	Hybrid Mass Damper (HMD)
2	Friction damper	High damping rubber bearings	Active Tendon Control System (ATCS)	Magnetorheological (MR) damper	Hybrid Base Isolator (HBI)
3	Tuned Mass Damper (TMD)	Elastomeric bearing	Multi Tuned Mass Damper (MTMD)	Piezoelectric Friction Damper (PFD)	
4	Tuned Liquid Damper (TLD)	Friction pendulum bearing	Active Tuned Mass Damper (ATMD)	Magnetorheological Elastomer (MRE)	
5	Viscoelastic damper		Electro-hydraulic Dampers (EHD)	Semi-active Tuned Mass Damper (SATMD)	

### Acknowledgments

This work supported by Research Program supported by the Department of Mechanical and Manufacturing Engineering. The authors would like to thank Universiti Putra Malaysia (UPM) and the Malaysian Ministry of Higher Education (MOHE) for their continuous support in the research work.

### References

- [1] Tavakolpour, Ali Reza, Intan Z. Mat Darus, Osman Tokhi, and Musa Mailah. "Genetic algorithm-based identification of transfer function parameters for a rectangular flexible plate system." *Engineering Applications of Artificial Intelligence* 23, no. 8 (2010): 1388-1397. <https://doi.org/10.1016/j.engappai.2010.01.005>
- [2] Crocker, M. J. "Handbook of Noise and Vibration Control." *John Wiley & Sons, Inc google schola* 2 (2007): 361-373. <https://doi.org/10.1002/9780470209707>
- [3] Dwivedy, Santosha Kumar, and Peter Eberhard. "Dynamic analysis of flexible manipulators, a literature review." *Mechanism and machine theory* 41, no. 7 (2006): 749-777. <https://doi.org/10.1016/j.mechmachtheory.2006.01.014>
- [4] Sayahkarajy, Mostafa, Z. Mohamed, and Ahmad Athif Mohd Faudzi. "Review of modelling and control of flexible-link manipulators." *Proceedings of the Institution of Mechanical Engineers, Part I: Journal of Systems and Control Engineering* 230, no. 8 (2016): 861-873. <https://doi.org/10.1177/0959651816642099>

- [5] Kotnik, Paul T., Stephen Yurkovich, and Ümit Özgüner. "Acceleration feedback for control of a flexible manipulator arm." *Journal of Robotic Systems* 5, no. 3 (1988): 181-196. <https://doi.org/10.1002/rob.4620050302>
- [6] Ge, Shuzhi Sam, Tong Heng Lee, and G. Zhu. "Genetic algorithm tuning of Lyapunov-based controllers: An application to a single-link flexible robot system." *IEEE Transactions on Industrial Electronics* 43, no. 5 (1996): 567-574. <https://doi.org/10.1109/41.538614>
- [7] Pereira, Emiliano, Sumeet S. Aphale, Vicente Feliu, and SO Reza Moheimani. "Integral resonant control for vibration damping and precise tip-positioning of a single-link flexible manipulator." *IEEE/ASME Transactions on Mechatronics* 16, no. 2 (2010): 232-240. <https://doi.org/10.1109/TMECH.2009.2039713>
- [8] Pereira, Emiliano, Sumeet S. Aphale, Vicente Feliu, and SO Reza Moheimani. "Integral resonant control for vibration damping and precise tip-positioning of a single-link flexible manipulator." *IEEE/ASME Transactions on Mechatronics* 16, no. 2 (2010): 232-240. <https://doi.org/10.1109/TMECH.2009.2039713>
- [9] Preumont, André. *Dynamics of electromechanical and piezoelectric systems*. Dordrecht, The Netherlands:: Springer, 2006.
- [10] Chen, Kaiwen, and Alessandro Astolfi. "Adaptive control for nonlinear systems with time-varying parameters and control coefficient." *IFAC-PapersOnLine* 53, no. 2 (2020): 3829-3834. <https://doi.org/10.1016/j.ifacol.2020.12.2560>
- [11] Talebi, Heidar A., Khashayar Khorasani, and Rajnikant V. Patel. "Neural network based control schemes for flexible-link manipulators: simulations and experiments." *Neural networks* 11, no. 7-8 (1998): 1357-1377. [https://doi.org/10.1016/S0893-6080\(98\)00038-0](https://doi.org/10.1016/S0893-6080(98)00038-0)
- [12] Donne, J. D., and U. Ozguner. "Neural control of a flexible-link manipulator." In *Proceedings of 1994 IEEE International Conference on Neural Networks (ICNN'94)*, vol. 4, pp. 2327-2332. IEEE, 1994. <https://doi.org/10.1109/ICNN.1994.374582>
- [13] Li, Hong-Xing, and CL Philip Chen. "The equivalence between fuzzy logic systems and feedforward neural networks." *IEEE Transactions on Neural Networks* 11, no. 2 (2000): 356-365. <https://doi.org/10.1109/72.839006>
- [14] Hu, Bao-Gang, George KI Mann, and Raymond G. Gosine. "A systematic study of fuzzy PID controllers-function-based evaluation approach." *IEEE transactions on fuzzy systems* 9, no. 5 (2001): 699-712. <https://doi.org/10.1109/91.963756>
- [15] Kim, Sang-Myeong, Heungseob Kim, Kwangsuck Boo, and Michael J. Brennan. "Demonstration of non-collocated vibration control of a flexible manipulator using electrical dynamic absorbers." *Smart Materials and Structures* 22, no. 12 (2013): 127001. <https://doi.org/10.1088/0964-1726/22/12/127001>
- [16] R. C. Hibbeler. "Engineering Mechanics – Dynamics." <https://www.academia.edu/43072240>
- [17] Shi, Shenghao, Dongxu Li, and Qing Luo. "Design and dynamic analysis of micro-vibration isolator for single gimbal control moment gyro." *Procedia Engineering* 99 (2015): 551-559. <https://doi.org/10.1016/j.proeng.2014.12.570>
- [18] Xu, Ruikun, Guoyuan Tang, De Xie, Daomin Huang, and Lijun Han. "Underactuated tracking control of underwater vehicles using control moment gyros." *International Journal of Advanced Robotic Systems* 15, no. 1 (2018): 1729881417750759. <https://doi.org/10.1177/1729881417750759>
- [19] Keshtkar, Sajjad, Jaime A. Moreno, Hirohisa Kojima, Kenji Uchiyama, Masahiro Nohmi, and Keisuke Takaya. "Spherical gyroscopic moment stabilizer for attitude control of microsatellites." *Acta Astronautica* 143 (2018): 9-15. <https://doi.org/10.1016/j.actaastro.2017.10.033>
- [20] Walker, Julie M., Heather Culbertson, Michael Raitor, and Allison M. Okamura. "Haptic orientation guidance using two parallel double-gimbal control moment gyroscopes." *IEEE transactions on haptics* 11, no. 2 (2017): 267-278. <https://doi.org/10.1109/TOH.2017.2713380>
- [21] Yang Yongtai. "Dynamic modeling, trajectory planning and vibration suppressing of the spatial flexible manipulators." *Beijing: Beijing Institute of Technology*. (2014).
- [22] Abbas Moloody, Azizan As'array, Tang Sai Hong, Mohd Sapuan Salit, Raja Kamil. "Modelling and Simulation the Position Control of Flexible Manipulator Using Gyroscopic Actuator." *ISASE published book*. (2021). <https://isase2021.atauni.edu.tr/wp-content/uploads/2021/05/ISASE2021V2.pdf>
- [23] Lee, Sangdeok, and Seul Jung. "Detection and control of a gyroscopically induced vibration to improve the balance of a single-wheel robot." *Journal of Low Frequency Noise, Vibration and Active Control* 37, no. 3 (2018): 443-455. <https://doi.org/10.1177/0263092317716075>
- [24] Tokhi, Mohammad Osman, and Abul KM Azad. "Design and development of an experimental flexible manipulator system." *Robotica* 15, no. 3 (1997): 283-292. <https://doi.org/10.1017/S0263574797000325>
- [25] Jovanović, Miroslav M., Aleksandar M. Simonović, Nemanja D. Zorić, Nebojša S. Lukić, Slobodan N. Stupar, and Slobodan S. Ilić. "Experimental studies on active vibration control of a smart composite beam using a PID controller." *Smart materials and structures* 22, no. 11 (2013): 115038. <https://doi.org/10.1088/0964-1726/22/11/115038>

- [26] Deif, Sarah, Mohammad Tawfik, and Hanan A. Kamal. "Vibration and position control of a flexible manipulator using a PD-tuned controller with Modified Genetic Algorithm." In *Proceedings of the ICCTA 2011 Conference*, pp. 15-17. 2011.
- [27] John, Subash, Abdul Imran Rasheed, and Viswanath K. Reddy. "ASIC implementation of fuzzy-PID controller for aircraft roll control." In *2013 International Conference on Circuits, Controls and Communications (CCUBE)*, pp. 1-6. IEEE, 2013. <https://doi.org/10.1109/CCUBE.2013.6718551>
- [28] Lakshmi, K. Vijaya, and P. Srinivas. "Fuzzy adaptive PID control of pitch system in variable speed wind turbines." In *2014 International Conference on Issues and Challenges in Intelligent Computing Techniques (ICICT)*, pp. 52-57. IEEE, 2014. <https://doi.org/10.1109/ICICT.2014.6781252>
- [29] Hadi, M. Sukri, Intan Z. Mat Darus, M. Osman Tokhi, and Mohd Fairus Jamid. "Active vibration control of a horizontal flexible plate structure using intelligent proportional–integral–derivative controller tuned by fuzzy logic and artificial bee colony algorithm." *Journal of Low Frequency Noise, Vibration and Active Control* 39, no. 4 (2020): 1159-1171. <https://doi.org/10.1177/1461348419852454>
- [30] JARAM: Journal of Advanced Research in Applied MECHANICS, Vol. 90 No. 1: February (2022) to Vol. 98 No. 1: October (2022), ISSN (Online): 2289 – 7895, *Akademia Baru Publishing (M) Sdn Bhd.* (2022). <http://www.akademiabaru.com/submit/index.php/aram>